Pergamon

*Int. J. Heat Mass Transfer.* Vol. 40, No. 17, pp. 4021–4030, 1997

Printed in Great Britain
0017–9310/97 $17.00 + 0.00

PII: S0017–9310(97)00077–X

# Effects of heater surface orientation on the critical heat flux—II. A model for pool and forced convection subcooled boiling

MATTHEW J. BRUSSTAR
Stirling Thermal Motors Inc, 275 Metty Drive, Ann Arbor, MI 48103-9444, U.S.A.

and

HERMAN MERTE, JR
The University of Michigan, Department of Mechanical Engineering and Applied Mechanics, 2250 G.G. Brown Laboratory, Ann Arbor, MI 48109-2125, U.S.A.

(*Received* 15 *February* 1996 *and in final form* 17 *February* 1997)

**Abstract**—A model for the critical heat flux (CHF) in pool and low-velocity forced convection boiling is proposed for heater surfaces relatively short in the flow direction, which utilizes an experimentally-observed relationship between the CHF and the bubble residence time for closure of the momentum and energy equations. The model is primarily concerned with describing the combined effects of heater surface orientation and flow on the CHF. Furthermore, it incorporates a convenient analytical means for including various other parametric influences, such as the bulk liquid subcooling and fluid property variations. A comparison of the model predictions with experimental results is given, showing reasonable agreement with the measured CHF for bulk liquid subcoolings ranging from 2.8 to 22.2 K, bulk flow velocities from 0.04 to 0.55 m $s^{-1}$ and heater orientations from zero to 360°. The present model represents an improvement over existing models for the effects of orientation in forced convection, and approaches the result of an earlier model for pool boiling. [Brusstar and Merte, Effects of buoyancy on the critical heat flux in forced convection. *AIAA Journal of Thermophysical Heat Transfer*, 1994, **8**(2), 322–328.] © 1997 Elsevier Science Ltd.

## INTRODUCTION

In Part I, the effect of buoyancy on the critical heat flux (CHF) in low-velocity forced convection was explicated. Previous interest in such work has arisen from many sources, among these microgravity boiling and microelectronics cooling. Early studies of buoyancy effects in forced convection boiling [1, 2] were conducted by varying the direction and magnitude of the flow velocity in heated vertical tubes. While these succeeded in identifying gravity-dependent and gravity-independent flow regimes for a specific set of conditions, a generalized criterion for distinguishing the two regimes was not developed. More recently, the effects of heater surface orientation and flow on the CHF for arrays of small heater sources have been studied by Gersey and Mudawar [3] demonstrating, as expected, the diminishing dependence of the CHF on orientation with increasing flow rates. A subsequent model to describe this dependence [4], based on heater surface rewetting due to an interfacial instability, succeeded in predicting a somewhat limited range of experimental data to within ±30%. The purpose of the present work is to address the shortcomings of these earlier works by presenting an improved means of modeling the effects of flow and heater surface orientation on the CHF, which thereby also provides a general means of predicting the transition to the so-called 'buoyancy-independent' limit of flow boiling. The CHF model is then extended to the limit of pool boiling as well, providing a result identical to that in an earlier work of Brusstar and Merte [5].

In the companion work, Part I, the product of the CHF and the bubble residence time, representing the energy per unit area leaving the heater surface during the bubble residence time, was identified as a key parameter in describing the CHF phenomenon. This product was found to be independent of the orientation of buoyancy, possibly due to its association with the evaporation in the thin liquid regions on the heater surface, where surface tension and viscous effects are expected to dominate [6]. The physical interpretation of the product of the CHF and bubble residence time can be obtained through an examination of its relation to earlier models of the CHF, including the macrolayer dryout model [7] and the hydrodynamic instability model [8]. Perhaps the most well-established of the pool boiling CHF correlations is that proposed by Zuber for a horizontal plate in a saturated liquid, given by:

**NOMENCLATURE**

| | |
|---|---|
| $A$ | area [m$^2$] |
| $c$ | virtual mass coefficient, specific heat [kJ kg$^{-1}$ K$^{-1}$] |
| $c_D$ | drag coefficient |
| $c_L$ | lift coefficient |
| $c_{pl}$ | specific heat of the liquid phase [kJ kg$^{-1}$ K$^{-1}$] |
| $D$ | bubble diameter [m] |
| $E''$ | product of CHF and bubble residence time [kJ m$^{-2}$] |
| $F$ | force [N] |
| $g$ | gravitational acceleration [m s$^{-2}$] |
| $h_{fg}$ | latent heat of evaporation [kJ kg$^{-1}$] |
| $Ja$ | Jakob number ($=\rho_l c_{pl}\Delta T_{sub}/\rho_v h_{fg}$) |
| $k$ | thermal conductivity [W m$^{-1}$ K$^{-1}$] |
| $L_H$ | heater length [m] |
| $p$ | pressure [N m$^{-2}$] |
| $q_c$ | CHF [kW m$^{-2}$] |
| $q_{co}$ | $q_z$ corrected for subcooling [equation (26)] [kW m$^{-2}$] |
| $q_z$ | CHF in saturated pool boiling predicted by Zuber's model [Equation (2)] [kW m$^{-2}$] |
| $q''$ | measured surface heat flux [kW m$^{-2}$] |
| $R$ | bubble radius [m] |
| $Re$ | Reynolds number based on hydraulic diameter |
| $s$ | bubble displacement [m] |
| $T_{in}$ | bulk temperature measured at the inlet to the test section [K] |
| $\Delta T_{sub}$ | bulk liquid subcooling [K] |
| $u$ | velocity component tangent to the heater surface [m s$^{-1}$] |
| $U_{bulk}$ | bulk flow velocity [m s$^{-1}$] |
| $\bar{U}_c$ | critical vapor velocity [m s$^{-1}$] |
| $v$ | velocity component normal to the heater surface [m s$^{-1}$] |
| $v'$ | volumetric rate of vapor generation [m$^3$ s$^{-1}$] |
| $V$ | bubble volume [m$^3$] |
| $x$ | bubble displacement tangent to the surface [m] |
| $y$ | bubble displacement normal to the heater surface [m]. |

Greek symbols

| | |
|---|---|
| $\chi$ | latent heat fraction, equation (10) |
| $\delta_o$ | liquid macrolayer thickness [m] |
| $\Phi$ | evaporation flux [m s$^{-1}$] |
| $\gamma$ | ratio of the area occupied by vapor stems to the total surface area |
| $\lambda$ | 'most unstable' Kelvin–Helmholtz wavelength [m] |
| $\lambda_\Gamma$ | 'most unstable' Rayleigh–Taylor wavelength [m] |
| $\theta$ | heater orientation angle [degrees] |
| $\rho$ | density [kg m$^{-3}$] |
| $\sigma$ | surface tension [kg s$^{-2}$] |
| $\tau$, $\tau_{res}$ | bubble residence time [s]. |

Subscripts

| | |
|---|---|
| B | body |
| c | CHF |
| k | iterative denoting of phase (liquid or vapor) |
| l | liquid |
| L | lift |
| meas. | measured value |
| pred. | predicted value |
| r | relative |
| s, S | surface |
| v | vapor, vapor stems |
| 0 | horizontal, facing-upward orientation. |

Superscripts

| | |
|---|---|
| * | at departure. |

$$q_z = \frac{\pi}{24}\rho_v h_{fg}^4 \sqrt{\frac{g\sigma(\rho_l-\rho_v)}{\rho_v^2}}. \quad (1)$$

Equation (1) is derived based on simple continuity arguments for vapor leaving the heater surface in the form of vapor jets spaced evenly on the heater surface, constrained by the Kelvin–Helmholtz stability criterion. Digressing from equation (1), the continuity of the vapor phase was given by Zuber in terms of the critical vapor velocity, $\bar{U}_c$, and the most unstable wavelength, $\lambda$, as follows:

$$q_c = \frac{\pi}{24}\rho_v \bar{U}_c h_{fg} = \frac{\pi}{24}\rho_v \left(\frac{\lambda}{\tau}\right) h_{fg}. \quad (2)$$

The above expression was considered to represent only the mean behavior of the vapor and accounted for no spacing between consecutive bubbles. In terms of the energy per unit area leaving during the bubble residence time, equation (2) may be written for the saturated case as:

$$E'' = q_c\tau^* = \frac{\pi}{24}\rho_v h_{fg}\lambda \sim \rho_v h_{fg} D^*. \quad (3)$$

$E''$ in this case is the enthalpy contained in the vapor bubbles formed between successive waves of length $\lambda$ and period $\tau$. This contrasts with the energy balance given in the macrolayer dryout models, in which $E''$ is

the enthalpy of evaporation contained in a uniform macrolayer of thickness $\delta_0$:

$$E'' = q_c\tau^* = \rho_l h_{fg}\delta_0(1-\gamma). \quad (4)$$

Relating the concepts of the two CHF models $E''$, therefore, represents a transference of energy from the evaporating thin liquid regions to the vapor bubbles. In terms of the product of which it is comprised, $E''$ is the energy leaving the heater surface during the period where the liquid is temporarily prevented from reaching the heater surface by the overlying vapor masses. Earlier studies of transition boiling [9, 10] suggest that at heat flux levels approaching the CHF, the increasing rate of evaporation on the heater surface gives rise to localized regions of film boiling, thereby resulting in an increasingly inefficient heat transfer process. Interpreted in this light, $E''$ represents the energy responsible for producing a dry area fraction on the heater surface sufficient to effect the transition to film boiling.

The hydrodynamic instability models introduce a mechanical energy limitation as the basic CHF mechanism; Haramura and Katto [7], on the other hand, were the first to associate the mechanical limit to the rate of vapor removal with a limit to the thermal energy in the thin liquid regions on the heater surface. In this respect, the macrolayer dryout model is similar to the present model, which links the mechanics of the vapor (manifested in the bubble residence time) with a limit to the thermal energy leaving the surface ($E''$). If the concept of a uniform macrolayer thickness were modified to represent an equivalent volume of vapor per unit area evaporated during the bubble residence time, then $E''$ would be equivalent to the heat of evaporation contained in the macrolayer. Viewed in this way, the concepts of $E''$ and $\delta_0$ differ only semantically, with both concepts being a progression in the analysis of the CHF from a purely mechanical energy limit, as in the hydrodynamic instability models [11], to a combined mechanical and thermal energy limit. The present model, however, refrains from the assumption of a uniform macrolayer and instead proposes $E''$ as a generalized concept to replace the macrolayer in a more physically accurate model of the CHF in pool and bubbly flow boiling.

## FORCED CONVECTION CHF MODEL DESCRIPTION

A model for the CHF is presented below, which primarily describes the effects of the bulk flow velocity and heater surface orientation. Also included is the effect of subcooling on the evaporation flux, which influences the bubble residence time as observed and presented in Part I. The model represents an initial attempt to describe the essential features of certain parametric influences observed in the laboratory, thereby giving reasonable quantitative agreement with experimental data. The present approach introduces two semi-empirical factors for model closure not used in previous works: $E''$, comprised of the product of the CHF and the bubble residence time and $\chi$, representing the fraction of the surface heat flux accounting for the growth of large bubbles.

*Description of bubble growth*

The largest bubbles are of primary significance in the present work, since they have been observed to predominate at high levels of heat flux [12] and are thought to play an important role in the dryout process by virtue of the amount of surface area they occupy [13]. While Kumada and Sakashita [14] observed three distinct sizes of bubbles at heat flux levels approaching the CHF, they also observed that the two smaller sizes among these tended to coalesce into the largest size. The discussion below is, therefore, limited to the growth of large bubbles.

The volume of a bubble is obtained through a spatial and temporal integration of the local evaporation flux, as follows:

$$V = \int_\tau \left( \int_{A_s} \Phi_V \, dA_s \right) dt. \quad (5)$$

Based on measurements of the volumetric growth rate of a bubble growing at high heat flux by Katto and Yokoya [15], it is assumed as a first approximation that the spatial integral of the evaporation flux, denoted $v'$, is temporally constant, such that:

$$V = v'\tau. \quad (6)$$

It may be noted that the use of $v'$ is a convenient means of describing the growth of the larger bubbles, accounting for both the evaporation at the base of the bubble and coalescence with neighbouring smaller bubbles. The vapor generation rate for the large bubbles is determined from the maximum possible vapor generation rate multiplied by the latent heat fraction, $\chi$:

$$v' = \chi\left(\frac{q_c A_s}{\rho_v h_{fg}}\right). \quad (7)$$

In the case of pool boiling over a horizontal surface, the unit surface area may be taken as the most unstable Taylor wavelength squared [7, 8]. While the CHF in pool boiling over a horizontal surface is independent of the heater size (provided the heater is not very small), it is expected that the heater length would affect the CHF for other orientations, except possibly in the case where $L/\lambda_T \sim 1$. A recent study of bubble growth on vertical and horizontal surfaces by Katto and Otokuni [16] suggests that for orientations other than horizontal, the unit surface area for the CHF in pool boiling may be given instead by:

$$A_s = \lambda_T \cdot L_H. \quad (8)$$

In the present model, however, consideration will be limited to heater surfaces whose length in the flow

direction is on the order of the most unstable Taylor wavelength. It is further assumed that the influence of relatively low flow velocities on the basic structure of the evaporating regions existing on the heater surface is negligible, allowing the characteristic surface area in equation (8) to be applied to low-velocity forced convection boiling as well. Accordingly, the expressions relating to the near-wall transport, including equation (7) and the correlation for the effect of subcooling to be presented below, will also be assumed applicable to low-velocity forced convection boiling.

*Subcooling effects*

In the experimental work described in Part I, it was found that the evaporation flux was reduced with increases in subcooling, slowing the rate of bubble growth for a given level of heat flux. If the fraction of energy responsible for evaporation is assumed to be unity, as is the case for the majority of previous pool boiling models, the model for bubble growth used by Haramura and Katto [7] yields bubble diameters far larger than those observed, especially for subcooled boiling. This fraction was found in Part I to be substantially less than unity and varied such that the volumetric rate of vapor generation at the CHF remained virtually independent of subcooling. If a reasonable bubble diameter at high levels of heat flux is assumed to be of the order of the most unstable Rayleigh–Taylor wavelength, then the volume of the bubble at departure is given as follows:

$$V^* \sim \lambda_T^3. \tag{9}$$

Assuming the process to occur far from the thermodynamic critical state, such that $\rho_v \ll \rho_l$, a generalized expression for the portion of energy associated with evaporation can be derived for subcooled boiling on dimensional grounds assuming buoyancy and virtual mass forces as:

$$\chi = \frac{c_0\left(\frac{\rho_v}{\rho_l}\right)^{1/2}}{\left(1+0.102\left(\frac{\rho_v}{\rho_l}\right)^{1/4} Ja\right)}. \tag{10}$$

Based on the measurements of the vapor generation rate with R113 given previously, $c_0 = 4.1$, varying about $\pm 20\%$ with orientation. In light of the 1/5-power dependence of the bubble residence time with $\chi$, to be demonstrated below, this variation is nonetheless of little significance. Given that $c_0$ is somewhat greater than unity, however, it is implied that equation (10) is valid only for cases where the density of the liquid phase is much greater than that of the vapor phase, as stated above.

*Heater surface orientation effects*

*I Forced convection boiling.* The kinematics of the vapor at CHF are described using a two-dimensional form of the two-fluid model. The general form of the equations of motion are given as:

$$\rho_k \frac{D\vec{u}_k}{Dt} = \vec{F}_{B,k} + \vec{F}_{S,k} - \vec{\nabla} p \tag{11}$$

where the subscript $k$ denotes either the liquid or vapor phase. As a first approximation, the two-phase pressure gradient is neglected, as are the changes in momentum of the liquid phase due to the interaction with the vapor. As such, the velocity of the liquid phase is assumed to obey law of the wall scaling typical of turbulent flow in ducts, given as [17]:

$$\begin{aligned} u^+ &= y^+ \quad y^+ < 5 \\ u^+ &= 2.5 \ln y^+ + 5.5 \quad 5 < y^+ < 70 \\ u^+ &= 8.74 (y^+)^{1/7} \quad y^+ > 70 \end{aligned} \tag{12}$$

where $u^+$ is the mean velocity non-dimensionalized with respect to the friction velocity and $y^+$ is the Reynolds number based on the friction velocity and the distance from the wall. For the vapor phase, the body force is retained along with the surface forces, consisting of the interfacial drag, lift and virtual mass acceleration. The density of the vapor is assumed much smaller than that of the liquid, so that the advective portion of the material derivative of the vapor can be assumed relatively small. Also, viscous shear and surface tension forces are neglected.

The body force acting on the vapor is given by:

$$\vec{F}_B = g(\rho_l - \rho_v) V \sin\theta \hat{i} + g(\rho_l - \rho_v) V \cos\theta \hat{j} \tag{13}$$

where $\hat{i}$ is tangent to the heater surface in the direction of imposed flow and $\hat{j}$ is normal to the heater surface, with the coordinate system origin placed at the site of origin of the bubble on the heater surface. The interfacial drag force is expressed as:

$$\vec{F}_D = \frac{1}{2} \rho_l C_D A_s u_r |u_r| \hat{i} \tag{14}$$

where the drag coefficient is assumed a function of the void fraction, using the relation given by Ishii and Zuber [18]. Their expression predicts that the drag coefficient is fairly constant for $\alpha < 0.7$, so $C_D$ is assumed to be 0.54, corresponding to $\alpha = 0.6$. The $\hat{j}$-component of the drag is neglected, since the motion normal to the heater surface is assumed irrotational. The interfacial lift force is given by:

$$\vec{F}_L = \frac{1}{2} \rho_l C_L A_s u_r^2 \hat{j}. \tag{15}$$

While the lift force for Stokes flow over a sphere is in the minus $\hat{j}$-direction, this is unrealistic due to slip at the liquid–vapor interface and the lift force is assumed to be directed away from the wall due to the Bernoulli effect. The lift coefficient is taken as 0.5 [19] for larger values of the Reynolds number based on bubble diameter and is assumed to follow the interpolation given by Klausner *et al.* [20] for lower Rey-

nolds numbers. The virtual mass force arises due to the acceleration of the vapor phase into the liquid phase in both the $\hat{i}$- and $\hat{j}$-directions. Also, the unsteady portion of the material derivative is included with the virtual mass acceleration for completeness in the formulation, although its contribution is ordinarily very small, yielding:

$$\vec{F}_{VM} = -\frac{d}{dt}((c_1\rho_l+\rho_v)Vu_v)\hat{i} - \frac{d}{dt}((c_2\rho_l+\rho_v)Vv_v)\hat{j}. \tag{16}$$

Here, $c_1$ and $c_2$ are constants determined from the virtual mass of a bubble moving tangent and normal to the heater surface, respectively. From classical hydrodynamic theory [21], the virtual mass of a spherical bubble moving parallel to the heater surface is 19/32 of the displaced liquid mass, while that for a bubble moving normal to the heater surface is 11/16 of the displaced liquid mass. It can be assumed for simplicity in the present model, however, that $c_1 \cong c_2 = c = 1/2$ with little detriment to the solution accuracy. It may be noted that the form of the virtual mass force in equation (16) implicitly assumes a quasi-steady velocity profile in the liquid phase, as in equation (12).

The momentum equation is then integrated twice, with respect to time, to yield the bubble displacement in the $\hat{i}$- and $\hat{j}$-directions. The total displacement of the center of mass of the bubble is then given by:

$$\|\vec{s}(\tau)\| = (x^2+y^2)^{1/2}. \tag{17}$$

At departure, the bubble radius is determined by assuming the outward velocity of the bubble interface due to evaporation to be equal to the buoyancy-induced velocity of the center of mass of the bubble, occurring where:

$$R^* = \|\vec{s}(\tau^*)\| = \left(\frac{3}{4\pi}v'\tau^*\right)^{1/3}. \tag{18}$$

This expression describes the inter-connection between the energy and momentum equations, as the right-hand side is derived from the energy equation in equation (7), while the left-hand side is derived strictly from the kinematics of the vapor phase. The final constraint placed on this expression to lend closure to the problem is the experimentally-confirmed relation between the bubble residence time and CHF, given as:

$$E'' = q_c\tau^* = \text{const.} \tag{19}$$

The value of $E''$ is selected to provide the best fit to the experimental data for each bulk flow velocity and subcooling.

*II Pool boiling (zero imposed flow).* The limit of pool boiling is an instructive case of the present model, as it lends itself to an explicitly analytical solution and, thereby, gives insight into the essential character of the present model at low flow velocities. In the limit of no imposed flow, the interfacial drag and lift forces become small in relation to the buoyancy and virtual mass acceleration forces. The flow around the growing bubble is assumed to be irrotational, interfacial viscous shear is neglected, since $\mu_l \gg \mu_v$ and the surface tension force of adhesion is assumed to be small relative to buoyancy. The momentum equation reduces to the following simple form, previously used by Davidson and Schueler [22] for air bubbles growing rapidly from an orifice in water and later extended to pool boiling at high heat fluxes by Haramura and Katto [7]:

$$\vec{g}(\rho_l-\rho_v)V = \frac{d}{dt}((m_{VM}+m_V)\vec{u}_v) \tag{20}$$

where $\vec{g} = g\sin\theta\hat{i} + g\cos\theta\hat{j}$. Equation (20) is then integrated twice with respect to time to yield the displacement of the center of mass of the growing bubble as:

$$\vec{s}(\tau) = \frac{g(\rho_l-\rho_v)}{(c_1\rho_l+\rho_v)}\sin\theta\frac{\tau^2}{4}\hat{i} + \frac{g(\rho_l-\rho_v)}{(c_2\rho_l+\rho_v)}\cos\theta\frac{\tau^2}{4}\hat{j}. \tag{21}$$

Then, for upward-facing orientations:

$$R^* = \frac{g(\rho_l-\rho_v)}{(c\rho_l+\rho_v)}\frac{\tau^{*2}}{4}. \tag{22}$$

Solving equation (22) for $\tau^*$ using equation (18), for the upward-facing case yields:

$$\tau^* = \left(\frac{3v'}{4\pi}\right)^{1/5}\left[\frac{4(c\rho_l+\rho_v)}{g(\rho_l-\rho_v)}\right]^{3/5}. \tag{23}$$

The volumetric rate of vapor generation can be determined using the expression for $\chi$ from equation (10) substituted into equation (7), yielding a prediction for the bubble departure time from equation (23) as well as the bubble departure radius from equation (22). The bubble departure diameters predicted from equation (22) for water and R113 are 31 and 8 mm, respectively, which is generally consistent with experimental data [23]. If both sides of equation (23) are multiplied by the CHF and it is assumed that the product of the CHF and the bubble residence time is independent of the effects of heater orientation, such that $E'' = q_c\tau^* = \text{const}$, then the CHF for upward-facing surfaces can be expressed as follows:

$$q_c = \left(\frac{E''}{\left(\frac{3\chi A_s}{4\pi}\right)^{1/5}\left[\frac{4(c\rho_l+\rho_v)}{g(\rho_l-\rho_v)}\right]^{3/5}}\right)^{5/6}. \tag{24}$$

For the case of highly wetting fluids, where the hydrodynamic instability model gives a reasonable prediction for the CHF, the value of $E''$ may be selected appropriately such that the CHF equals that predicted for pool boiling over a horizontal surface [8] corrected for subcooling [24]:

$$q_c = q_z\left(1+0.102\left(\frac{\rho_v}{\rho_l}\right)^{1/4} Ja\right) = q_{co}. \quad (25)$$

For downward-facing heater surfaces, the displacement component normal to the surface is neglected, since the buoyancy force normal to the heater is balanced by the reaction force of the wall, giving the downward-facing complement to equation (23) as follows:

$$\tau^* = \left(\frac{3v'}{4\pi}\right)^{1/5}\left[\frac{4(c\rho_l+\rho_v)}{g(\rho_l-\rho_v)\sin\theta}\right]^{3/5} \quad (26)$$

which, correspondingly, yields the CHF for the downward-facing orientations as

$$q_c = q_{co}\,|\sin\theta|^{1/2}. \quad (27)$$

Equations (25) and (27) are identical to the model of the effects of heater orientation given originally in a previous work [1] and successfully compared with experimental data at low flow velocities in Fig. 5 of Part I, despite the fact that the present model is based on an entirely different set of assumptions. The two models, however, are similar in that they assume that a critical amount of liquid is brought to the surface and subsequently evaporated, hence the agreement. A comparison of equations (25) and (27) with experimental data from other works is given in the earlier work cited above, with reasonable agreement.

As an aside, the mean CHF for large convex surfaces can be estimated through integration of equations (25) and (27) over the heater surface with respect to the orientation angle. Such an analysis tacitly assumes that the radius of curvature of the surface is larger than the characteristic bubble size and convex surfaces are assumed in order to preclude consideration of bubble crowding effects associated with concave surfaces. Integration of equations (25) and (27) along the surface gives a mean CHF of $0.881q_{co}$ for a long cylinder and $0.937q_{co}$ for a large sphere, which compares somewhat favorably with the predictions of $0.889q_{co}$ and $0.866q_{co}$, respectively, by Lienhard and Hasan [11].

## COMPARISON WITH EXPERIMENTAL RESULTS

The forced convection CHF data presented in this section were acquired using the experimental apparatus and procedures described in Part I. The only change to the apparatus description is the test section height, which was changed as needed from 12.7 to 3.2 mm to attain a wider range of bulk flow velocities. The heater surface orientation designations are identical to those in Fig. 3 of Part I, with the horizontal, upward-facing orientation assumed as zero degrees and between zero and 180° denoting upflow and 180–360° denoting downflow. The CHF values, meanwhile, are non-dimensionalized with respect to the CHF predicted for pool boiling corrected for subcooling [equation (25)]. This does not necessarily imply similarity with pool boiling, but is instead used to provide a well-known reference with which to compare the CHF results for low-velocity forced convection boiling.

Figure 1 shows a comparison of the CHF model predictions with measurements for a bulk flow velocity of 0.18 m $s^{-1}$, which approaches the buoyancy-dominant or pool boiling limit. The data exhibit only small deviations from the behavior expected for pool boiling and the model shows very little effect of the flow forces except in the case of downflow, where the flow forces oppose the buoyancy force. Figure 2 shows the model predictions for the ratio of the buoyancy force parallel to the heater surface to the drag force acting on the bubbles at the moment of departure as a function of the heater surface orientation for a flow velocity of 0.18 m $s^{-1}$. The predicted ratio of the buoyancy to the lift force for these flow conditions is also included, indicating that the lift is insufficient to overcome buoyancy except at orientations close to the vertical downflow position. In addition, the buoyancy and drag forces at departure appear to be similar in magnitude, but opposite in sign in downflow, which explains the experimentally-observed tendency of the vapor to stagnate above the heater surface. Moreover, this near-balance of buoyancy and drag in the downflow orientations causes the CHF to be particularly sensitive to marginal increases in the drag force due to the local acceleration of the liquid in the test section associated with the relatively high rates of vapor production. This secondary effect, precluded from the present model by assuming a steady velocity profile, is especially prominent due to the relatively small flow channel area and may account for the deviation of the experimental data from the model predictions for downflow.

A comparison of the CHF model with experimental

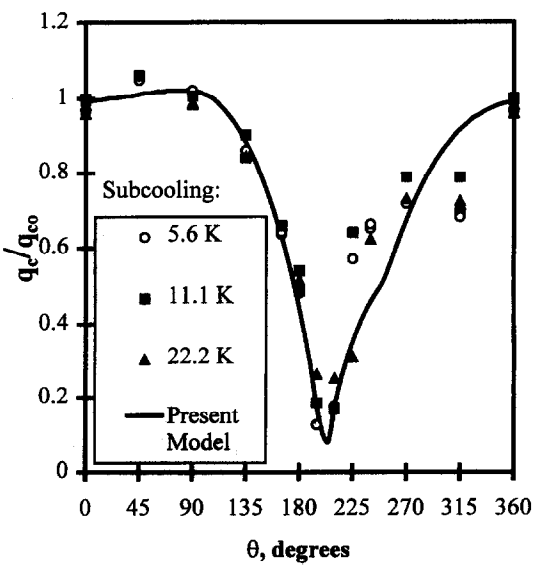


Fig. 1. Comparison of the measured CHF with the present model predictions as a function of orientation; test conditions: $U_{bulk} = 0.18$ m $s^{-1}$; $Re = 3400$; test section height = 3.2 mm; $T_{in} = 322$ K.

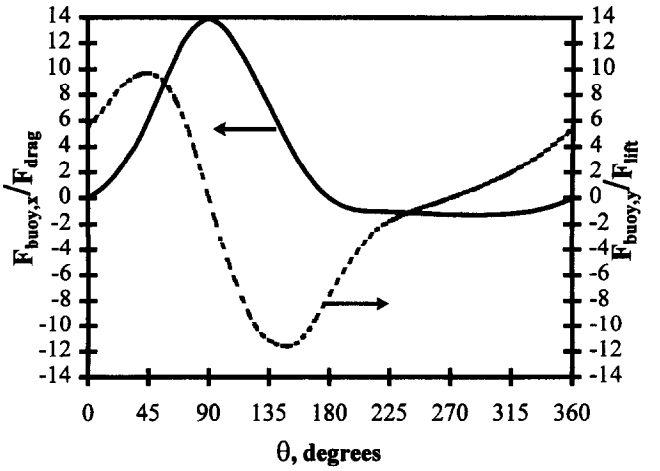


Fig. 2. Model predictions for the ratio of the buoyancy force components parallel and normal to the heater surface acting on a bubble at departure compared with the respective drag and lift forces: $U_{bulk} = 0.18$ m s$^{-1}$.

data at $U_{bulk} = 0.32$ m s$^{-1}$ in Fig. 3 shows a greater effect of the flow forces on the CHF. Overall, there appears to be good quantitative agreement between the CHF model and the experimental data, especially for the higher levels of subcooling. As compared with pool boiling, the minimum CHF is shifted from the horizontal down orientation to one slightly inclined, with buoyancy acting opposite the imposed flow. The model predictions for the ratio of the buoyancy force acting opposite the drag force as well as the ratio of the buoyancy force acting opposite the lift force are shown at bubble departure as a function of heater orientation in Fig. 4, showing that the drag and lift forces acting on the vapor at departure are approximately equal in magnitude and opposite in sign to the buoyancy force in the downward-facing orientations with downflow. As such, the vapor has a strong tendency to stagnate above the heater surface, thereby increasing the probability for coalescence between neighboring bubbles, particularly for the present case in which the lift force is expected to be somewhat balanced by the reaction force of the bubbles against the wall of the test section opposite the heater surface. Visual observations confirm the prevalence of coalescence and the resulting oversized vapor slugs depart upstream against the imposed flow, where they would gradually collapse and, subsequently, recirculate over the heater surface. Combined with the suppression of the lift force, the recirculation of vapor over the heater surface serves to lower the CHF in the downflow orientations, despite the competing influence of the local bulk flow acceleration on the CHF noted in Fig. 2 for $U_{bulk} = 0.18$ m s$^{-1}$. Notwithstanding these secondary effects, the first-order model still appears to give a reasonable estimate of the CHF at all heater orientations for $U_{bulk} = 0.32$ m s$^{-1}$.

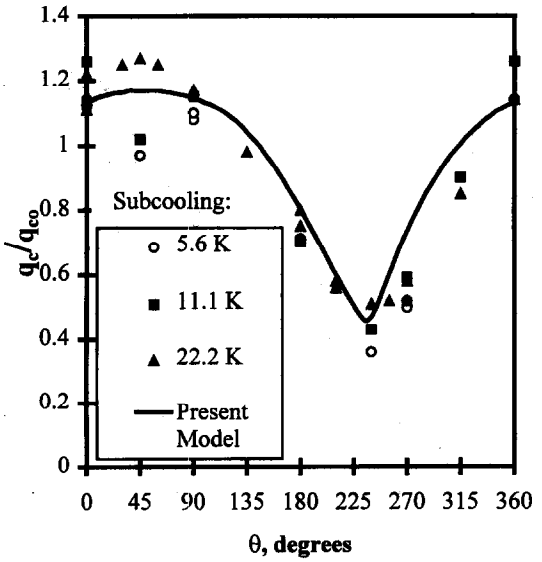


Fig. 3. Comparison of the measured CHF with the present model predictions as a function of orientation; test conditions: $U_{bulk} = 0.32$ m s$^{-1}$; $Re = 6300$; test section height = 3.2 mm; $T_{in} = 322$ K.

Figure 5 shows a comparison of CHF measurements with the model predictions as a function of orientation for various subcoolings and a bulk flow velocity of 0.55 m s$^{-1}$. The flow forces in this case generally dominate over the buoyancy force, as evidenced by the relatively small difference in the CHF between the two vertical orientations. Also, the difference between the minimum and maximum CHF values in the figure lies nearly within $\pm 20\%$ of one another, indicating that the threshold of the buoyancy-independent flow boiling regime is being approached. Again, in spite of some relatively small deviations from the model predictions for downflow (likely resulting from the suppression of the lift force), the experimental results agree well with the forced convection model, particularly at higher subcoolings.

A direct comparison of the experimental data with the model predictions is given in Fig. 6 for heater orientations ranging from zero to 360°, subcoolings from 2.8 to 22.2 K and bulk flow velocities from 0.04

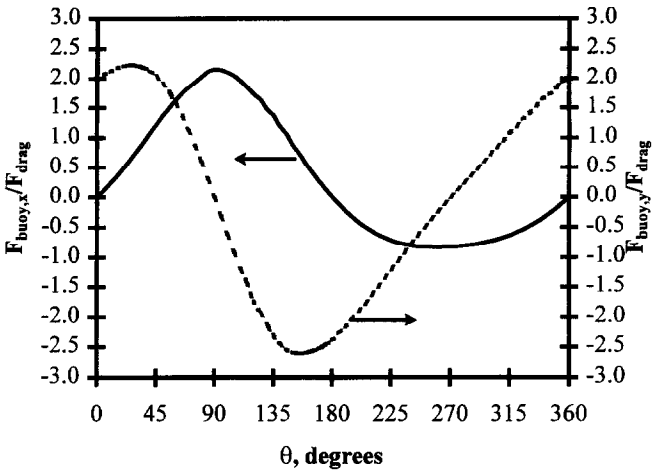


Fig. 4. Model predictions for the ratio of the buoyancy force components parallel and normal to the heater surface acting on a bubble at departure compared with the respective drag and lift forces: $U_{bulk} = 0.32$ m s$^{-1}$.

to 0.55 m s$^{-1}$. The presentation in this form tends to emphasize those data which deviate most from the model predictions, in contrast to the more meaningful trends represented in Figs 1, 3 and 5 above. While most of the 269 data points fall well within the generous ±30% tolerance band indicated, a few points, mostly those for downflow conditions, deviate substantially more. This is due primarily to the failure of the present model to account for the accumulation of vapor in the narrow test section with downflow at lower subcoolings, which is discussed below. These deviations do not significantly diminish the overall accuracy of the model, however, whose RMS error in predicting these data is estimated at ±10%.

## DISCUSSION

The ability of the present forced convection model to predict the CHF in the limits of pool boiling and nearly buoyancy-independent forced convection boiling demonstrates features that are common to both regimes. Besides the model for bubble growth and motion used for both the pool and low-velocity forced convection boiling, the inverse proportionality between the CHF and the bubble residence time was also successfully applied to both pool and forced convection boiling. In an earlier work, Haramura and Katto [7] attempted to extend the macrolayer and vapor stem model to low-velocity forced convection boiling, therefore, agreeing with the present work in

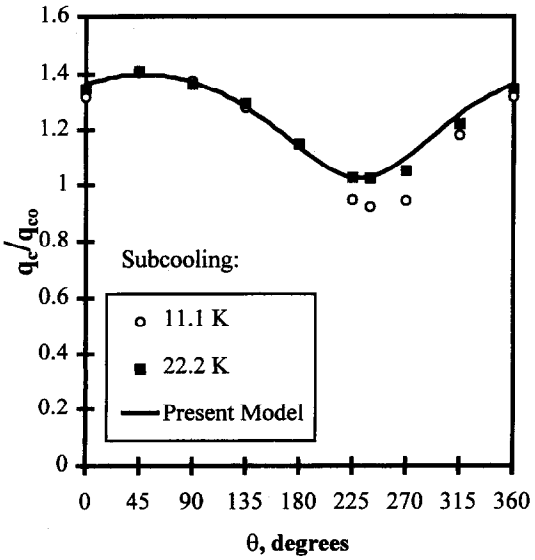


Fig. 5. Comparison of the measured CHF with the present model predictions as a function of orientation; test conditions: $U_{bulk} = 0.55$ m s$^{-1}$; $Re = 10\,500$; test section height = 3.2 mm; $T_{in} = 322$ K.

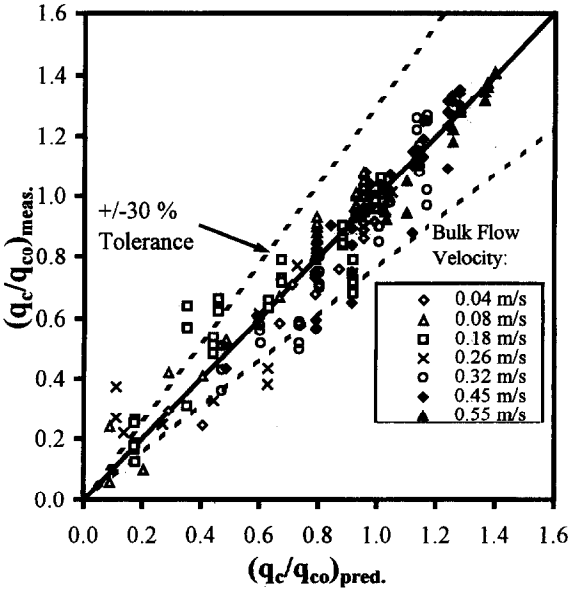


Fig. 6. Comparison of the measured CHF with the present model predictions for bulk flow velocities ranging from 0.04 to 0.55 m s$^{-1}$ and subcoolings ranging from 2.8 to 22.2 K.

one important aspect: both assume the thin evaporating domains characteristic of pool boiling at high heat fluxes to be largely uninfluenced by an imposed bulk flow velocity. $E''$, however, while analogous in many respects to the macrolayer, differs from the macrolayer in that $E''$ was found to decrease approximately with the square root of the flow velocity [25], perhaps as a result of shear thinning in the evaporating domains. The present model nonetheless is similar to the macrolayer and vapor stem model of Haramura and Katto [7] in that it provides a CHF mechanism that is independent of gravity orientation and applicable to pool and low-velocity forced convection boiling.

The CHF data presented here demonstrate a transition from buoyancy-dominance at low flow velocities to near buoyancy-independence at high flow velocities. Consistent with the findings of Papell [2], the threshold of the buoyancy-independent regime appears to be largely a function of the bulk liquid subcooling, as the CHF for the downflow orientations in Figs 3 and 5 are noted to be particularly sensitive to changes in subcooling. Conversely, the forced convection model presented here, which does not consider the acceleration of the bulk flow due to vapor production nor the recirculation of vapor due to condensation upstream, predicts no such effect of bulk liquid subcooling. This discrepancy perhaps indicates that increasing the bulk liquid subcooling mitigates the confinement of the uncondensed vapor by the test section which, although generally a secondary effect, can become significant to the CHF. The effect of the channel height is also witnessed in the work of Gersey and Mudawar [4], where the test section height of 5 mm was slightly smaller than the expected bubble departure size of 8 mm. As a result, the effect of subcooling on their CHF measurements for downflow is described somewhat poorly by the correlation represented by equation (25) and used in the present work. However, such flow channel geometry effects are not general to all boiling problems and, therefore, are not useful in defining a general limit to the buoyancy-independent flow boiling regime. In the absence of such flow channel effects, the model predictions in Fig. 5 for a bulk flow velocity of 0.55 m $s^{-1}$ indicate that the CHF is expected to vary by less than $\pm 20\%$ with orientation, showing that the CHF for R113 closely approaches the buoyancy-independent limit.

Completely apart from flow channel geometry and local void accumulation effects, the effect of the bulk liquid subcooling on the CHF is characterized reasonably well by the correlation by Ivey and Morris [24] for pool boiling. The measurements of the volumetric rate of vapor generation given in Part I suggest that this effect arises due to the decrease in the percent of the total heat flux resulting in evaporation. The consequences of this apparent reduction in the proportion of thin film heat transfer are that the dependence of the CHF on the secondary parameters normally associated with thin film dynamics is smaller than would otherwise be expected were evaporation the dominant mode of heat transfer. One particular example is the effect of surface wettability and surface roughness. Surface factors, normally small, have been found in extreme cases to produce as much as a 20–30% change in the CHF [26], which is still somewhat less than would be expected were thin film evaporation beneath the large bubbles the dominant mode of heat transfer. While some progress in modeling surface effects has been made [27], such models generally remain fixed to the assumption of vapor stems with a microlayer at the base, which differs substantially from the physical portrayal of boiling at high heat fluxes presented in Part I. Another example is the effect of the heater surface material properties, where the large local temperature gradients associated with thin film evaporation produce a dependence of the CHF on the 'thermal conpacitance', $k\rho c$ [28]. The ratio of the thermal conpacitance for copper compared with that for quartz is over 100, yet the ratio of the CHF measured for thick copper surfaces vs quartz was only 0.60, perhaps also indicative of the relatively small portion of the total heat flux that is accounted for by the evaporation in the thin liquid regions. The muted effects of the secondary parameters that are linked closely with thin film evaporation, including viscosity, gives further validation for the model of subcooling given by equation (26).

The success of the present model to describe the influence of flow, orientation and subcooling suggests that the essential physical characteristics of the process have been incorporated. The present approach, however, has several as yet unresolved limitations. First, the value of $E''$ used for closure of the energy and momentum equations must be determined empirically, as no means is yet available for predicting its value for a generalized set of test conditions and for various test fluids. The model is thus somewhat restrictive, but does provide a conceptual means of injecting various parametric effects while remaining completely separate from the assumptions of a uniform liquid macrolayer and vapor stems. Second, by not implying a definite physical structure for the heat transfer regions on the heater surface, the concept of $E''$ is not as convenient of a modeling tool as the macrolayer. On the other hand, the present model refrains from suggesting a configuration that is not in keeping with photographs and physical observations.

## CONCLUSIONS

A simplified two-fluid model has demonstrated reasonable agreement with experimental data for relatively short heater surfaces in the flow boiling regime ranging between the lower limit of pool boiling and the upper, buoyancy-independent limit. The following conclusions may be drawn:

(1) As expected, the dependence of the CHF on the heater surface orientation diminishes with increasing flow velocity. For low flow velocities ($U_{bulk} < 0.08$ m

$s^{-1}$), the CHF approaches the predictions for pool boiling, and depends strongly on the heater orientation in the downward-facing positions. For high flow velocities ($U_{bulk} > 0.55\ m\ s^{-1}$), on the other hand, the CHF varies only by about $\pm 20\%$ with orientation, indicating a transition to the buoyancy-independent flow regime.

(2) The concept of $E''$, the energy transferred from the heater surface during the bubble residence time, is forwarded as a physically meaningful CHF mechanism and is consistent with earlier models of the CHF. Assuming the value of $E''$ to be independent of the heater orientation appears valid over the range of flow rates utilized in the present work, suggesting a similarity in the CHF mechanisms for pool boiling and low-velocity forced convection boiling.

(3) The effect of subcooling is modeled such that the volume of vapor produced at CHF is independent of subcooling for a given orientation and flow velocity. Apart from the secondary effects of the flow channel geometry and local void accumulation on the CHF, the effects of subcooling correlate reasonably well with the prediction for pool boiling given by Ivey and Morris [24].

*Acknowledgements*—This work was funded in part under NASA grants NAG3-1310 and NGT-50928, for which the authors express their gratitude.

## REFERENCES

1. Papell, S. S., Buoyancy effects on forced-convective boiling. ASME Report 67-HT-63, 1967.
2. Simoneau, R. J. and Simon, F. F., A visual study of velocity and buoyancy effects on boiling nitrogen. NASA TN D-3354, 1966.
3. Gersey, C. O. and Mudawar, I., Orientation effects on critical heat flux from discrete, in-line heat sources in a flow channel. *Transactions of the ASME, Journal of Heat Transfer*, 1993, **115**(4), 973–985.
4. Gersey, C. O. and Mudawar, I., Effects of heater length and orientation on the trigger mechanism for near-saturated flow boiling critical heat flux—II. Critical heat flux model. *International Journal of Heat and Mass Transfer*, 1995, **38**, 973–985.
5. Brusstar, M. J. and Merte Jr, H., Effects of buoyancy on the critical heat flux in forced convection. *AIAA Journal of Thermophysical Heat Transfer*, 1994, **8**(2), 322–328.
6. Bankoff, S. G., Dynamics and stability of thin heated liquid films. *Transactions of the ASME, Journal of Heat Transfer*, 1990, **112**(3), 538–546.
7. Haramura, Y. and Katto, Y., A new hydrodynamic model of critical heat flux, applicable to both pool and forced convection on submerged bodies in saturated liquids. *International Journal of Heat and Mass Transfer*, 1983, **26**, 389–399.
8. Zuber, N., On the stability of boiling heat transfer. *Transactions of the ASME, Series C, Journal of Heat Transfer*, 1958, **80**(4), 711–720.
9. Ishigai, S. and Kuno, T., Experimental study of transition boiling on a vertical wall in open vessel. *Bulletin of JSME*, 1966, **9**(34), 361–368.
10. Dhuga, D. S. and Winterton, R. H. S., Measurement of surface contact in transition boiling. *International Journal of Heat and Mass Transfer*, 1985, **28**, 1869–1880.
11. Lienhard, J. H. and Hasan, M. M., On predicting boiling burnout with the mechanical energy stability criterion. *Transactions of ASME, Journal of Heat Transfer*, 1979, **101**(2), 276–279.
12. Gaertner, R. F., Photographic study of nucleate pool boiling on a horizontal surface. *Transactions of ASME, Series C, Journal of Heat Transfer*, 1965, **88**(1), 17–29.
13. Kirby, D. B. and Westwater, J. W., Bubble and vapor behavior on a heated horizontal plate during pool boiling near burnout. *Chemical Engineering Progress Symposium Series, Heat Transfer*, 1965, 238–248.
14. Kumada, T. and Sakashita, H., Pool boiling heat transfer—II. Thickness of liquid macrolayer formed beneath vapor masses. *International Journal of Heat and Mass Transfer*, 1995, **38**, 979–987.
15. Katto, Y. and Yokoya, S., Principal mechanism of boiling crisis in pool boiling. *International Journal of Heat and Mass Transfer*, 1968, **11**, 993–1002.
16. Katto, Y. and Otokuni, S., Behavior of vapor masses on a vertical flat surface of comparatively large height near critical heat flux conditions in saturated pool boiling. *International Journal of Heat and Mass Transfer*, 1994, **37**, 255–263.
17. Schlichting, H., *Boundary-Layer Theory*, 7th edn. McGraw-Hill, New York, 1979, pp. 602–609.
18. Ishii, M. and Zuber, N., Drag coefficient and relative velocity in bubbly, droplet or particulate flows. *AIChE Journal*, 1979, **25**(5), 843–855.
19. Auton, T. R., The lift force on a spherical body in a rotational flow. *Journal of Fluid Mechanics*, 1987, **183**, 199–218.
20. Klausner, J. F., Mei, R., Bernhard, D. M. and Zeng, L. Z., Vapor bubble departure in forced convection boiling. *International Journal of Heat and Mass Transfer*, 1993, **36**, 651–662.
21. Milne-Thomson, L. M., *Theoretical Hydrodynamics*, 3rd edn, Macmillan, New York, 1956, pp. 476–479.
22. Davidson, J. F. and Schueler, B. O. G., Bubble formation at an orifice in an inviscid liquid. *Transactions of the Institution of Chemical Engineers*, 1960, **38**, 144–154.
23. McFadden, P. W. and Grassman, P., The relation between bubble frequency and diameter during nucleate pool boiling. *International Journal of Heat and Mass Transfer*, 1962, **5**, 169–173.
24. Ivey, H. J. and Morris, D. J., On the relevance of the vapour–liquid exchange mechanism for subcooled boiling heat transfer at high pressure, UKAEA, AEEW-R 137, 1962.
25. Brusstar, M. J., Relative effects of flow and orientation on the critical heat flux in subcooled forced convection boiling. Ph.D. thesis, University of Michigan, 1995.
26. Liaw, S. P. and Dhir, V. K., Void fraction measurements during saturated pool boiling of water on partially wetted vertical surfaces. *Transactions of the ASME, Journal of Heat Transfer*, 1989, **111**(3), 731–738.
27. Dhir, V. K. and Liaw, S. P., Framework for a unified model for nucleate and transition pool boiling. *Transactions of the ASME, Journal of Heat Transfer*, 1989, **111**(3), 739–746.
28. Carvalho, R. D. M. and Bergles, A. E., The effects of the heater thermal conductance/capacitance on the pool boiling critical heat flux. *Proceedings of the Engineering Foundation Conference on Pool and External Flow Boiling*. ASME, New York, 1992, pp. 2–17.